Correlation between micromagnetism and tunnel magnetoresistance in magnetic tunnel junctions using artificial ferrimagnets

C. Tiusan, T. Dimopoulos, K. Ounadjela, Michel Hehn, H. van den Berg, V. da Costa, Y. Henry

Correlation between micromagnetism and tunnel magnetoresistance in magnetic tunnel junctions using artificial ferrimagnets

C. Tiusan, T. Dimopoulos, and K. Ounadjela
Institut de Physique et de Chimie des Matériaux de Strasbourg (IPCMS), 23 rue du Loess, F-67037 Strasbourg Cedex, France

M. Hehn
Laboratoire de Physique des Matériaux, UMR CNRS 7556, Université H. Poincare F-54506, Nancy, France

H. A. M. van den Berg
Siemens AG, ZT MF1, Paul Gossenstrasse 100, Erlangen D-91052, Germany

V. da Costa and Y. Henry
Institut de Physique et de Chimie des Matériaux de Strasbourg (IPCMS), 23 rue du Loess, F-67037 Strasbourg Cedex, France
(Received 1 June 1999; revised manuscript received 20 September 1999)

The impact of the micromagnetic configuration on transport properties of magnetic tunnel junctions is presented. An artificial ferrimagnet system (AFi), made of two ferromagnetic layers with different magnetic moments antiferromagnetically coupled by exchange interactions through a Ru spacer layer, is used as a hard magnetic subsystem of the magnetic junction. Magnetic-force microscopy studies have shown that the magnetization reversal in artificial ferrimagnet systems occurs through the formation of Néel-type 360° domain walls. The stability of these walls is demonstrated to be different in the two magnetic layers of the AFi. These aspects have major effects in magnetic tunnel junction devices, due to the extreme sensitivity of spin tunneling to spatial variations in local magnetic order. The large tunnel magnetoresistance (TMR) of our samples, in the range of 20–30 % at room temperature, makes the tunnel junctions highly sensitive to magnetic fluctuations. A sharp switching of the soft magnetic layer upon field reversal prevents a domain structure from occurring in the soft magnetic layer, in the field window used for our micromagnetic studies. The tunnel device can thus be used as a sensitive probe for measuring small magnetic fluctuations associated with micromagnetic defects, domains, and walls in the AFi system. These fluctuations modulate the resistance of the tunnel junction and are fully reflected in the shape and the amplitude of the TMR signal.

I. INTRODUCTION

Spin-polarized tunneling in magnetic tunnel junctions, made of alternating layers of magnetic metals and insulators, has attracted much attention since the discovery of large tunnel magnetoresistance (TMR) at room temperature.[1] This effect relates to the fact that quantum tunneling of electrons between two ferromagnetic electrodes separated by a thin insulator is a spin-dependent phenomenon. The tunneling probability of electrons and therefore the resistance of a tunnel junction is controlled by the relative orientation of the magnetization in its ferromagnetic electrodes. In practice, this requires a pair of electrodes for which the orientation of each magnetization can be reversed independently. Commonly, a magnetically hard-soft system is used for this purpose. While the methods used to obtain the soft layer are quite the same, they differ significantly for the hard layer. Growth-induced uniaxial anisotropy or exchange biasing a ferromagnetic layer using an antiferromagnetic layer have been extensively used to fix the magnetization of the hard layer.[2] However, uniaxial anisotropies are difficult to control and the rigidity of exchange-biased films shows in general a rapid decrease when increasing temperature.

We report here an alternative way to harden a magnetic film by using an artificial ferrimagnet subsystem (AFi) made of two ferromagnetic layers with different magnetic moments, antiferromagnetically coupled by an exchange interaction through a nonmagnetic spacer. The main advantages of such hard subsystems are the large thermal stability (up to 250 °C) and the high coercive field of the net magnetization (up to 0.6 kOe) achieved by varying the thickness of the two magnetic layers, these two features being of essential importance for potential sensor applications. A large number of the combination of metals gives rise to the appearance of an oscillatory antiferromagnetic coupling,[3–9] but only a few are suitable for such applications. The antiferromagnetic coupling strength must be as large as possible in order to duplicate the domain structure of one layer in the other. As will be shown in this paper, this is the key factor to pin the largest magnetic moment against rotation and in this way to increase the magnetic rigidity. Since the highest coupling strength has been measured in Co/Ru/Co (Ref. 6) and Co/Rh/Co sandwiches,[10,11] our choice has turned towards the use of Ru as a spacer.

This paper is devoted to the examination of the field-dependent micromagnetic behavior of Ru-based artificial ferrimagnets and the analysis of the consequences on the transport properties in magnetic tunnel junctions which use this AFi as a magnetic hard layer. A systematic analysis of the magnetic properties of the constituent layers (the single layers) reveals that the behaviors of the two AFi magnetic layers, during the magnetization process, are substantially dif-

ferent. Besides the different shapes of the magnetoresistance (MR) curves as a function of the stacking sequence of the constituent layers, the overall shape of the MR loop can be explained within our model. A microscopic study of the domain structure of the AFi subsystem by magnetic-force-microscopy (MFM) gives insights on the magnetization processes responsible for the magnetization reversal. Evidence is given that reversal occurs through irreversible antiphase domain structure,[9] which gives rise to Néel-type 360° domain walls after rotation of the magnetization in each domain. We demonstrate that these generated walls persist after the reversal has occurred up to higher field values in the thin layer than in the thick layer. The source of wall pinning relates to the fluctuation of the exchange coupling between the two ferromagnetic layers. The correlation between macroscopic transport measurements and the microscopic distribution of magnetization shows that the presence of a domain structure leads to the appearance of different resistance channels and therefore has a direct consequence on the TMR signal.

In this paper, we present a comprehensive analysis of the correlation between micromagnetics and tunnel transport in magnetic systems that use the artificial ferrimagnet. The paper is organized as follows: Sec. II provides information on growth conditions and fabrication of the tunnel junctions as well as discussion of the importance of the stack design and the quality of the tunnel barrier, which is critical for the transport properties. In Sec. III, the concept of the artificial ferrimagnet is explained and described using macroscopic magnetization and transport measurements. Results are compared with experiments on single layers to illustrate the additional source of wall pinning associated with the exchange coupling and the consequences on the magnetic rigidity. In Sec. IV, the micromagnetic structure of both single layers and coupled layers is described, supported by magnetic-force microscopy experiments under magnetic field. We describe the formation of the domain structure and the occurrence of Néel-type 360° walls. In Sec. V, we illustrate the impact of the domain structure on the tunnel magnetoresistive signal. We emphasize the presence of 360° walls, further supported by the tunneling transport experiments, and we discuss in detail the stability of those walls which are formed in the artificial ferrimagnet.

II. MULTILAYER FILM PREPARATION AND EXPERIMENTS

A. Growth and study of the buffer layer

Since quantum tunneling between metal electrodes through an insulating barrier is known to be strongly dependent on the morphology of the metal-insulator interfaces, much effort has been put into optimizing the flatness of these interfaces. To ascertain the quality of the interfaces, we have optimized the growth of a complex buffer layer which leads to AFi subsystem with characteristics close to those achieved in high quality molecular-beam epitaxy (MBE) grown samples.[6,12]

The entire growth of the multilayer film was done *in situ*, in a high vacuum alliance concept sputtering system having a base pressure of 2×10^{-8} mbar. Figure 1(a) shows a typical layer sequence with the stack of a Cr/Fe/Cu buffer layer on

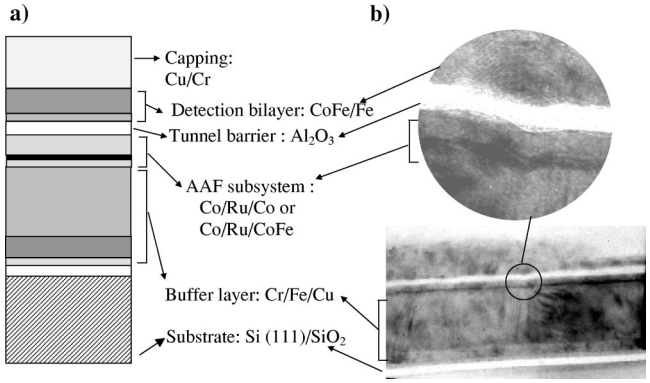

FIG. 1. (a) Magnetic tunnel junction (MTJ) stack design: Si(111)/Cr(1.6 nm)/Fe(6 nm)/Cu(30 nm)/Co(1.8 nm)/Ru(0.8 nm)/Co(3 nm) or CoFe(3 nm)/Al_2O_3(1.5 nm)/CoFe(1 nm)/Fe(6 nm)/Cu(10 nm)/Cr(5 nm). (b) Transmission electron microscopy (TEM) cross section image of the MTJ stack.

Si(111), a Ru-based AFi subsystem (Co/Ru/Co or Co/Ru/CoFe), an Al_2O_3 tunnel barrier, a CoFe/Fe detection bilayer, and a Cu/Cr capping bilayer.

Reproducible characteristics of the magnetic active layers have been achieved by first growing a Cr(1.6 nm)/Fe(6 nm)/Cu(30 nm) buffer layer on a previously sputter-etched 3 inch diameter Si(111) wafer. The topographic and magnetic properties of the magnetic active part of each sample have been optimized as a function of Cu and Fe thickness. As a preliminary, changes in the topography of the surface of the buffer and topmost AFi Co or CoFe layer were studied as a function of the Fe and Cu layer thickness, using *ex situ* atomic-force microscopy (AFM). The buffer roughness was found to decrease with increasing Fe thickness and decreasing Cu thickness. The addition of a Cr seed layer, necessary to obtain a higher coercivity of the AFi magnetic layers, reinforces this trend. The best compromise was obtained by setting the thicknesses of the Cr, Cu, and Fe to 1.6, 6, and 30 nm, respectively. The 30 nm Cu layer ensured a small resistance of the bottom current lead of the junctions (buffer layer) as compared to the resistance of the barrier in the final sensor devices,[13] as well as a magnetic decoupling of the Fe seed layer and AFi structure. A thickness of 6 nm of Fe was sufficient to achieve a suitable buffer smoothness, while introducing a parasitic magnetic signal sufficiently small so as not to hinder the interpretation of the magnetization curves recorded on the complete junction stacks.

By using such Cr/Fe/Cu buffer layers, a reasonable surface roughness of the hard subsystem topmost layer was achieved (peak to peak and rms values of 8 and 1.8 Å, respectively), irrespective of the Ru and Co or CoFe layer thickness. Notice that a significant increase of the surface roughness was eventually observed after the formation of the Al oxide layer on top of the AFi subsystem. The peak to peak and rms roughness then reached 13 and 3 Å, respectively.

B. Growth and study of the tunnel barrier and the magnetic soft layer

The Al oxide barrier was formed using the oxidation technique developed by Greiner.[14] This technique allows the oxi-

dation process to be carried out within a standard commercial sputtering plant without the need of accessing a separate chamber having a glow discharge plasma source. An Al layer is first deposited on top of the AFi subsystem. The substrate table then serves as a cathode for generating a rf Ar/O_2 plasma. A competition thus occurs at the Al surface between sputter etching by Ar ions and oxidation by oxygen ions, which leads to a self-limited oxidation process. In this study, the rf power density was set to 0.05 W/cm^2, the partial pressure of both Ar and O_2 gases to 9×10^{-3} mbar, and the oxidation time was optimized by x-ray photoelectron spectroscopy experiments to obtain fully oxidized Al barriers for a given thickness of the as-deposited Al (details can be found in Ref. 15). The optimization of the oxidation time is an extremely important step, in order to avoid over and under oxidation of the barrier, both known to result in detrimental effects on the magnetic tunel junction (MTJ's) magnetotransport properties.[16]

A magnetically soft system was sputtered on top of the Al oxide tunnel barrier. The so-called detection bilayer (DL) used in our MTJ, consisting of $Co_{50}Fe_{50}$ (1 nm)/Fe(6 nm) bilayers have a coercive field smaller than 20 Oe, driven mainly by the 6 nm thick Fe layer. The CoFe layer increases the electron polarization in the magnetic layer adjacent to the oxide barrier. In agreement with the Julliè re model,[17] an enhancement of the TMR signal is expected by the use of a CoFe mixture because of the larger spin polarization of CoFe compared to Co (larger average magnetic moment of Co in CoFe).

The multilayer stack shown in Fig. 1(a) is illustrated by a cross section transmission electron microscopy (TEM) image in Fig. 1(b). It gives an insight on the MTJ multilayer sequence, with a zoom on the Al oxide tunnel barrier. The TEM image indicates that the small roughness observed *ex situ* by AFM is conserved after depositing the rest of the stack. Furthermore, it shows that the roughness of the layers is correlated (corrugation of interfaces) as illustrated by the TEM image [Fig. 1(b)]. Roughness-induced large fluctuations in the thickness of the different layers are therefore avoided, leading to high quality tunnel barrier without pinholes which would act as hot conduction points.

In order to perform tunnel transport measurements, the as-deposited 3 inch wafers, containing the stack described above, were patterned in four UV lithography-etching steps into large arrays of junctions with square-shaped tunnel barrier of nominal surface areas $S=10\times10$, 20×20, and 50×50 μm^2. Detailed information on the wafer processing is described elsewhere.[18] The junctions were measured at room temperature[15] using a conventional four-point technique with a dc voltage source.

The magnetic properties of the as-deposited multilayer films were studied at both macroscopic and microscopic scales. The macroscopic magnetization curves were measured using an alternating gradient field magnetometer at room temperature. At a microscopic scale, the domain structure has been observed using a magnetic-force microscope (MFM) in zero and finite in-plane applied fields up to $|H|=600$ Oe. The MFM setup consists of a *Nanoscope Dimension 3100* equipped with a magnetic CoCr coated Si tip, magnetized along the tip axis. The scans have been performed at about 30 nm above the surface in the tapping-lift (interlace) mode developed by Digital Instrumental. This mode allows us to disentangle the long-range magnetic and the short-range topographic information during the same image acquisition. Since the detected signal (frequency shift of the vibrating cantilever) is proportional to the second derivative of the local field, this technique provides a good signal-to-noise ratio.

III. MACROSCOPIC MAGNETIC PROPERTIES

The use of the artificial ferrimagnetic structures as hard subsystems in a tunnel junction device requires the understanding of its magnetic response when submitted to an external applied field. The artificial ferrimagnet consists of an asymmetric trilayer stack composed of two Co or Co and CoFe layers of different thicknesses, both layers being antiferromagnetically coupled by exchange interaction through a nonmagnetic spacer layer. The top layer is thicker and has therefore a larger moment m_1, than the bottom layer with moment m_2. In this work, Ru has been used as a spacer layer mainly due to its high coupling strength.[12] The magnetic layers consist of either pure cobalt layers (Co/Ru/Co) or Co and CoFe (Co/Ru/CoFe) which allow us to investigate a large range of gain in rigidity, as will be shown in the proceeding sections (III A, III B). The antiferromagnetic (AF) coupling of both systems shows similar coupling strength as well as an oscillatory behavior as a function of Ru thickness (t_{Ru}), with maxima at $t_{Ru}=3$ Å and $t_{Ru}=8$ Å, the signature of interface quality comparable to MBE grown samples.[6,5,12,19] In this study, a Ru layer thickness of 0.8 nm has been used to increase the thermal stability of the AFi and avoid the presence of a biquadratic coupling that exists for Ru thicknesses in the range of 4–6 Å.[12]

A. Magnetic macroscopic properties of an artificial ferrimagnet

The room-temperature magnetization of a typical AFi system: Buffer/Co(1.8 nm)/Ru(0.8 nm)/Co(3 nm)/Al_2O_3(2 nm) is shown in Fig. 2(a). The insets describe the relative orientation of the magnetic moments at different fields along a decreasing field branch from the positive saturation field ($+H_s$) to the negative saturation field ($-H_s$). The topmost arrow gives the net magnetic moment orientation of the thick Co layer, m_1, the middle arrow the thin Co layer m_2, and the bottom arrow the Fe layer included in the buffer layer m_{Fe}. Decreasing the field from $+H_s$ saturation, a first hysteresis appears in the flank region in a field range varying from 4–2 kOe [Fig. 2(a)]. This hysteresis is attributed to the development of a domain structure during the reversal of the thin AFi layer[9] with the smallest magnetic moment (m_2). The net magnetic moment remains oriented along the applied positive field. Consequently, the magnetic moment of the thick AFi layer (m_1) remains oriented along the positive field while the magnetic moment of the thin AFi layer (m_2) reverses to be oriented opposite to the field. Furthermore, since the magnetic layers are polycrystalline, the local sense of rotation of the magnetic moments inside a layer can be influenced by thermal activation, small inhomogeneities of local exchange interactions or local anisotropy. Therefore, regions spaced far enough to overcome the exchange

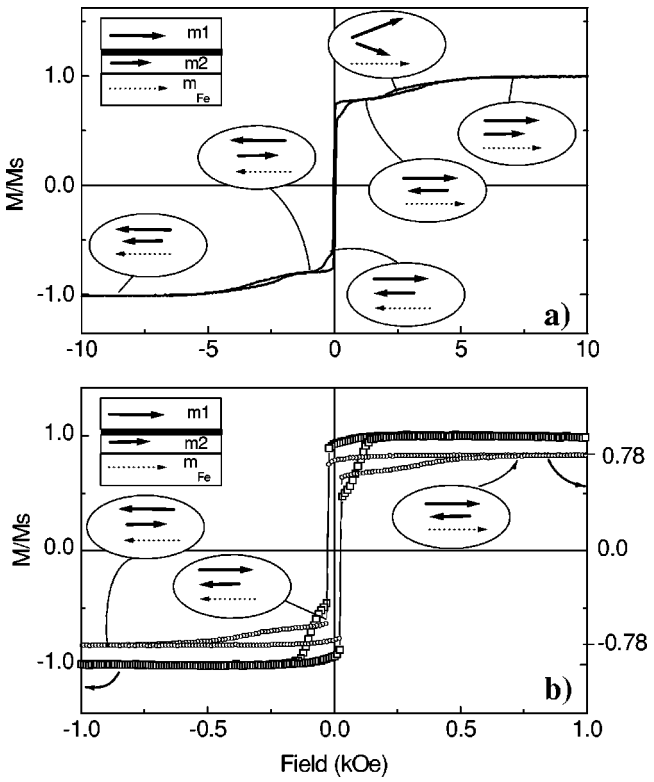

FIG. 2. (a) Magnetization curve of a typical AFi subsystem: buffer / Co(1.8 nm) / Ru(0.8 nm) / Co(3 nm) / Al_2O_3. (b) Zoom on the AFi magnetization curve (± 1 kOe) ($-\bigcirc-$) and comparison with the magnetization curve of a single cobalt layer made on the same conditions ($-\square-$).

interactions will rotate clockwise or counterclockwise, leading to the appearance of magnetic domains when decreasing the applied field. By further decreasing the applied field, the domain structure in the thin magnetic layer, and therefore this hysteresis, disappears and the M-H curve shows a plateau for which the net magnetization remains constant. $H_p = 1.5$ kOe measures the width of the plateau in a positive field (Fig. 2). On the plateau, the magnetizations of both magnetic layers are strongly antiferromagnetically coupled and each layer is uniformly magnetized. The width of the plateau is given by the following expression:[20]

$$H_p = (m_1 - m_2)/(m_1 + m_2)H_s . \quad (1)$$

This width defines the operational field window of the tunnel device using the AFi subsystem. Therefore, we focus our investigation on minor loops for applied fields $-H_p \leqslant H \leqslant +H_p$. In a negative applied magnetic field, the Fe layer switches first abruptly at 20 Oe followed by the continuous reversal of the net magnetization of the AFi. This reversal is completed when the net moment $(m_1 - m_2)$ is oriented along the negative field direction, giving rise to a plateau in the negative side of the curve. On this plateau, the magnetic moments of both magnetic layers are again mutually firmly antiferromagnetically coupled. The gain in rigidity, induced by the AF coupling of the two magnetic layers of the AFi system is given[20] by the ratio Q [total magnetic moment at saturation over net magnetic moment at the plateau, i.e., $Q = (m_1 + m_2)/(m_1 - m_2)$]. This theoretically predicted gain in rigidity is experimentally verified by comparing the coercive fields of the AFi ($\simeq 400$ Oe) and the single cobalt layer ($\simeq 100$ Oe) [Fig. 2(b)]. The rigidity of a single magnetic layer stems from the frictional torque against rotation, originated from the microscopic (local) anisotropy of the randomly oriented crystallites that constitute the layers. The layers do not exhibit any pronounced macroscopic magnetic anisotropy in the plane of the films. As shown in Fig. 2(b), the AFi amplifies[21] the magnetic rigidity of a single magnetic layer that enters in its structure by the factor Q (here $Q \simeq 3$). Consequently, the magnetic properties (i.e., coercivity) of the single magnetic layer strongly determine the rigidity of the AFi. Therefore, the larger the coercivity of the single layer, the better the magnetic response of the AFi for the use as a hard layer. The next paragraph describes the best conditions used to achieve a large coercivity for the single magnetic layers of the AFi.

B. Magnetic macroscopic properties of a single Co and CoFe magnetic layers

The macroscopic M-H loops of a buffer/Co(3 nm) single layer covered by 3 nm of Ru were studied. As a buffer layer, we have used the optimized Cr(1.6 nm)/Fe(6 nm)/Cu(30 nm). The switching of the Fe buffer corresponds to the steep change of M at low fields (20 Oe) and is not further discussed (Fig. 3). The corresponding hysteresis loop shows a gradual reversal of the Co layer, with a coercive field of about 100 Oe, in contrast to a steep switching and a larger coercivity for a Co layer grown on the same buffer but covered with Cu, for which the coercive field is about 250 Oe [Fig. 3(a)]. It appears that by capping with Ru, the softening of the Co layer was caused by the interfacial mixing between Co and Ru. Several explanations converge towards the idea that at the interface, Ru is strongly intermixed with Co in comparison with a very low intermixing degree in the case of Co/Cu.[22] Due to the granular structure of Co, Ru can diffuse between the grains at the interface and decrease the magnetic thickness and the exchange coupling between the grains. The chemical affinity of these elements tends to mix the interface, independently of the deposition technique. The intermixed region is over 3 ML at each interface.[12]

To overcome the magnetic consequences of intermixing in the case of Co and Ru, we have added Fe in the Co layer since Fe and Co show a large chemical affinity being totally miscible. Due to a higher chemical affinity between Co and Fe than between Co and Ru, the mixing of the $Co_{50}Fe_{50}$/Ru interface has been strongly reduced. An experimental proof is given in Fig. 3(a) where the magnetization curves of the $Co_{50}Fe_{50}$ sample capped with Ru seem to be identical to those of the Co capped with Cu. Indeed, the coercive field is high (more than 220 Oe), 2 to 3 times higher than in Co/Ru layers grown on the same buffer layer and the magnetization reversal is much sharper. Moreover, a systematic study of magnetization versus thickness of a pure CoFe film capped with Ru has shown that only half of a monolayer is magnetically dead at the interface while more than two atomic layers are magnetically dead for pure Co capped with Ru.

The advantage of building Co/Ru/$Co_{50}Fe_{50}$ artificial ferrimagnets instead of Co/Ru/Co is related to the larger coercivity of $Co_{50}Fe_{50}$ compared to the coercivity of a single Co layer capped with Ru. In this way a large rigidity of the AFi

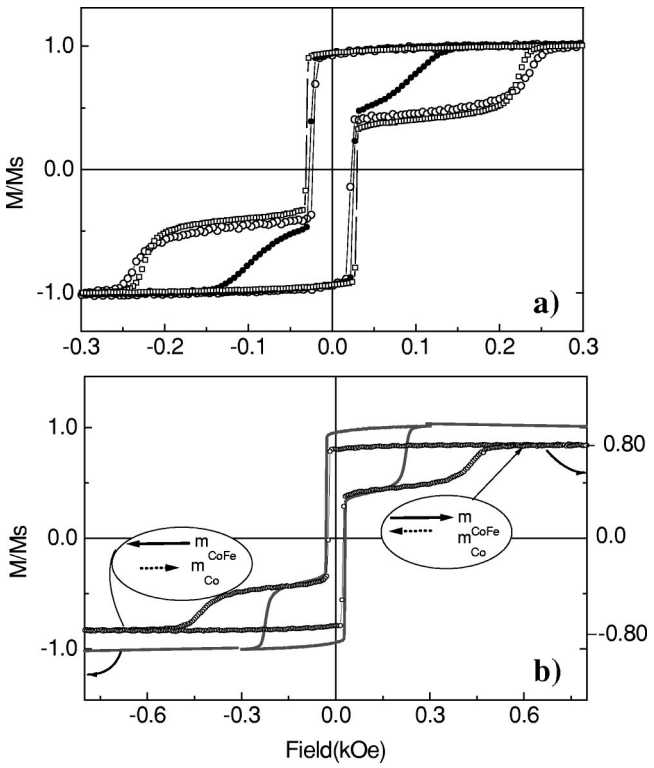

FIG. 3. (a) Magnetization curve of single Co(3 nm) layer sputtered on Si(111)/Cr(1.6 nm)/Fe(6 nm)/Cu(30 nm) buffer layer capped with Ru ($-\bullet-$) and Cu ($-\ \bigcirc\ -$). The $Co_{50}Fe_{50}$ (3 nm) capped with Ru, sputtered on the same buffer layer, has similar properties ($-\square-$) with the cobalt single layer capped with Cu. (b) Magnetization curve for Co(2 nm) / Ru(0.8 nm) / $Co_{50}Fe_{50}$ (3 nm) AFi in a field range of ± 1 kOe ($-\bigcirc-$) by comparison with the single $Co_{50}Fe_{50}$ (3 nm) layer performed under the same conditions ($---$). The experimental enhancement of rigidity gives a factor ($Q_{exp}=2$).

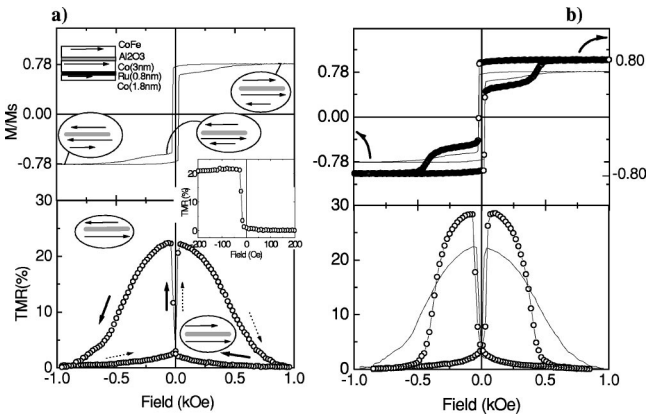

FIG. 4. (a) Magnetization curve of a typical Co/Ru/Co/Al_2O_3/CoFe/Fe stack ($---$) in a field range of ± 1 kOe, correlated with the TMR curve ($-\bigcirc-$). (Inset) Minor TMR loop for the detection layer in a field range where the AFi acts as a rigid block. (b) Influence of the AFi magnetic properties on the TMR signal shape and amplitude. The MH and corresponding TMR curves for the MTJ having $Co_{50}Fe_{50}$ as the top layer of the AFi interfaced with the tunnel barrier ($-\bigcirc-$) differ in shape and amplitude from the corresponding case when the top layer of the AFi system is Co ($---$). *M-H* curves are measured on planar (reference) films, grown in the same sputtering run with the wafers used for patterning junctions.

can be achieved by a smaller amplification factor *Q*. Indeed, as shown in Fig. 3(b), the rigidity of Co/Ru/CoFe with $Q_{exp}=2$ is similar to the one observed for the Co/Ru/Co system with $Q_{exp}=3$. This has strong effects in the domain structure developed during the magnetization reversal, as we will be shown in the next paragraph.

C. Transport properties of MTJ using the artificial ferrimagnet as a hard magnetic layer

We have investigated in detail the two following magnetic tunnel junctions, for which the only difference is the topmost AFi magnetic layer: S_1: [*hard subsystem* Co/Ru/Co]/Al_2O_3/[*soft bilayer* CoFe/Fe] and S_2: [*hard subsystem* Co/Ru/CoFe] / Al_2O_3 / [*soft bilayer* CoFe/Fe]. The *M-H* and corresponding TMR loops for S_1 and S_2 [shown in Figs. 4(a) and 4(b)] measured in the operational field window of the tunnel device, demonstrate the influence of the magnetic behavior of the hard subsystem on the shape of the TMR signal. In the positive part of the plateau [Fig. 4(a) corresponding to Co/Ru/Co/Al_2O_3/CoFe/Fe tunnel junction], the detection bilayer and the topmost (thick) layer of the AFi are aligned along the field direction. Consequently, a parallel configuration of magnetization for the layers adjacent to the barrier induces a high probability of tunneling and so a small resistance of the MTJ. By reversing the applied magnetic field, the detection bilayer reverses its magnetization inducing an antiparallel configuration responsible for a high resistance of MTJ. This antiparallel state is preserved as long as the net magnetic moment of the AFi, (m_1-m_2), remains rigid and oriented along the positive field direction. As soon as the reversal of the net moment (m_1-m_2) is completed, the magnetization of the topmost layer of the AFi becomes again parallel with the detection bilayer giving rise to a small resistance of the MTJ device. The shape and the amplitude of the TMR signal are modified by using the Co/Ru/$Co_{50}Fe_{50}$ AFi as a magnetic hard layer in the MTJ device, as shown in Fig. 4(b). One of the significant advantages of using $Co_{50}Fe_{50}$ at the interface with the tunnel barrier is that the amplitude of the TMR signal is enhanced from 22% to 30%, due to the higher spin polarization at the $Co_{50}Fe_{50}$/oxide interface. Particularly important is that the antiparallel state does not give a flat plateau in the TMR curve as shown in Fig. 4(a). This confirms that the AFi system is not a fully magnetically homogeneous and rigid block but consists of domains which start to develop in negative field. The difference in shape of the TMR curves for the Co/Ru/$Co_{50}Fe_{50}$ AFi stems from differences in the reversal characteristics of this hard subsystem in comparison with Co/Ru/Co.

The reversal process as well as the signal height is controlled by the field-dependent micromagnetic structure of the two coupled magnetic layers. Understanding this requires a detailed analysis of local MFM features together with correlation of the *MR* curves, which is the purpose of the next section.

IV. MICROSCOPIC MAGNETIC PROPERTIES

Models for magnetization reversal rely on the well-known ripple domain configuration in thin magnetic films.[23–28] The

Co and CoFe alloy layers are polycrystalline and are made of small magnetic grains coupled by exchange interactions. On a macroscopic scale, the layers are magnetically isotropic due to a random orientation of the easy magnetic axis of each grain. However, on a microscopic scale an effective local anisotropy can be defined as well as an effective correlation, where the length scale is characterized by the exchange correlation length l_{ex}. This correlation length is very sensitive to spatial variations of the anisotropy, to the magnetic moment, and the coupling strength between grains and to thermal fluctuations. Therefore, a spatial fluctuation of l_{ex} is expected over the layer surface. The coupling strength depends on the thickness of the magnetic film.[28] Micromagnetic calculations show that for small thicknesses and weakly coupled grains, the reversal of the layer magnetization proceeds by rotation of the individual grain magnetic moments. A characteristic ripple structure starts to appear when either the thickness or the coupling between the grains is increased.[28]

A. Magnetic microscopic properties of a single layer

The magnetization reversal for a $Co_{50}Fe_{50}$(3 nm) single layer covered with Ru is illustrated in Fig. 5 using a magnetization curve and a set of corresponding MFM images obtained at specific applied fields. By reducing the external field from positive saturation to zero, dark and bright contrasts corresponding to magnetic charge accumulations begin to form, consistent with randomly distributed small fluctuations of the magnetization orientation relative to the field axis direction. This domain structure is created by independent rotation of magnetization from site to site as we proceed from saturation towards zero applied field. When the field is reversed, the moments inside uniformly magnetized regions weakly coupled with the neighboring regions will rotate first, in agreement with the increase of contrast in the MFM image [Fig. 5(b)]. Then, increasing the negative field, the magnetization inside the tightly coupled regions will start to rotate. When regions with a different sense of rotation of their local magnetization meet, correlated Néel walls start to establish as shown from the fine correlated structures which appear on Fig. 5(c). As the negative field further increases, the neighboring moments are dragged in the field direction by exchange interactions, increasing the effective length of the 360° Néel walls, as evidenced in the MFM images Figs. 5(d) and 5(e). Appendix A shows that the MFM signal is consistent with the stray fields for a 360° wall. The walls remain pinned at fields higher than fields for which the reversal of the magnetization in domains is almost completed. This is shown in Fig. 5(e), where isolated stable 360° walls are still present despite the absence of charge accumulation within the regions separated by the walls, (absence of contrast) indicating that in domains the magnetization is fully aligned along the direction of the field. This unstable situation (the center of the wall has its magnetization oriented oppositely to the field) is overcome at fields of 300 Oe, large enough to allow the wall to escape from the pinning centers [Fig. 5(f)]. The distribution of depinning fields is consistent with the gradual disappearance of the 360° walls observed in the MFM images.

These reversal features are sketched in Fig. 6. The figure shows a model for the evolution of the magnetic moment

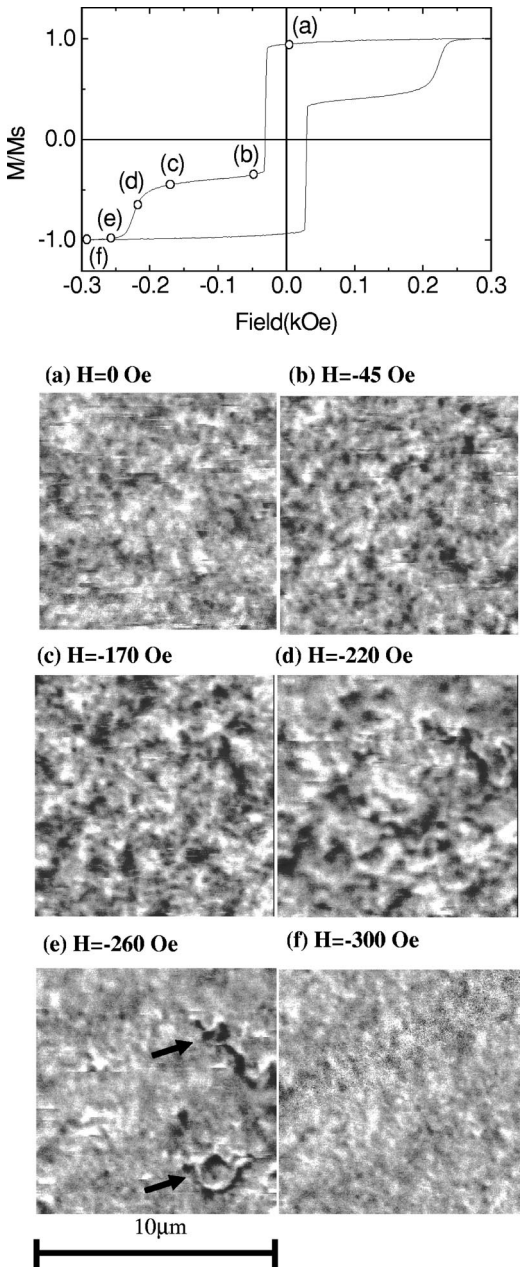

FIG. 5. A successive set of MFM images for buffer/$Co_{50}Fe_{50}$ (3 nm) magnetization reversal at some significant magnetic-field values, indicated on the attached M-H curve: (a) 0 Oe, (b) −45 Oe, (c) −170 Oe, (d) −220 Oe, (e) −260 Oe, (f) −300 Oe. During the reversal connected Néel walls appear. Black arrows point linear and circular isolated stable 360° walls.

distribution in uniformly magnetized regions, as a function of a negative applied field H. The clockwise rotation of the bottom left moment m_{bl}, and counterclockwise rotation of the bottom right moment m_{br}, give rise to a region where the torque is compensated and therefore the magnetic moment of this center region m_{bc} remains along the positive saturating field direction [Fig. 6(a)]. With the increase of the negative applied field, the rotation of m_{br} and m_{bl} proceeds and leads to the appearance of two 180° winding Néel type walls [Fig. 6(b)]. Since the lateral extension of m_{bc} (shaded region in the figures) does not exceed the size of the 180° walls, the magnetization rotates continuously from the m_{bc} to the m_{bl} di-

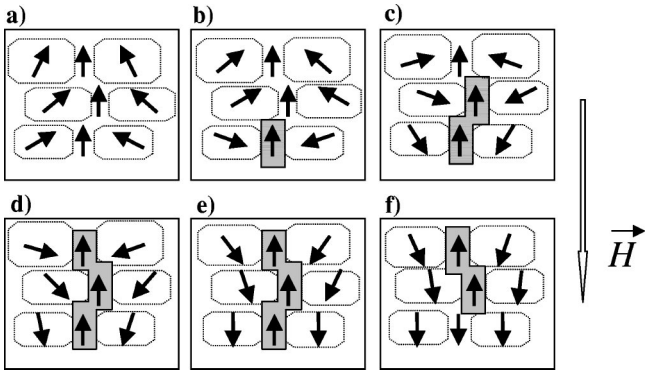

FIG. 6. Sketch showing how connected Néel walls are formed during reversal in a negative magnetic field. In an AFi system, each magnetic moment has its antiferromagnetic image mirrored in the other magnetic layer, due to the strong AF coupling.

rection. Therefore, the region separating m_{bc} from m_{bl} can be described as a single 360° winding Néel-type wall where the center is ascribed to m_{bc}. As the negative field increases, the neighbor moments will be dragged in the field direction by exchange interactions. Consequently, correlated 360° Néel walls will form increasing the effective wall length as sketched in Figs. 6(c) and 6(d). After the reversal is completed, for fields larger than the local pinning fields, walls or segments of walls disappear [Fig. 6(f)].

B. Magnetic microscopic properties of the artificial ferrimagnet system

As shown in the previous section (IV A), the competition between the local anisotropies and the exchange interactions govern the development of the domain structure in single magnetic films. In the AFi system, the AF coupling between the two magnetic layers adds an *additional* contribution to the nucleation and stability of the domain structure. Indeed, roughness-induced variations in the Ru spacer thickness produce inhomogeneities in the AF coupling distribution that hinder a rotation in unison of the layer's magnetization and act as nucleation and wall pinning centers). Consequently, the density of walls increases in comparison with a single layer and their stability under a reversed applied field is enhanced by the AF coupling. These assumptions are supported by the field-dependent microscopic magnetic analysis in two AFi's with different net moment, Co(1.8 nm)/Ru(0.8 nm)/Co(3 nm) and Co(2 nm)/Ru(0.8 nm)/$Co_{50}Fe_{50}$(3 nm). Figure 7 compares the MFM images of these two systems, measured at characteristic field values. The results allow us to analyze the field-dependent magnetic properties of an artificial ferrimagnet when decreasing its net magnetic moment. Similarly to the single magnetic layers, when decreasing the field from saturation, uniformly magnetized regions appear, whose effective magnetic moments are aligned within an angle bisected by the direction of the positive saturation field. The MFM contrast of the remanent state (not shown) is then similar to the one observed in a single CoFe layer [Fig. 5(a)]. When reversing the field the moments inside the areas presenting the smallest coupling (direct lateral exchange coupling and indirect AF interlayer coupling) will rotate first. The sense of rotation of the moments is determined by the local effective anisotropy. Increasing the negative field

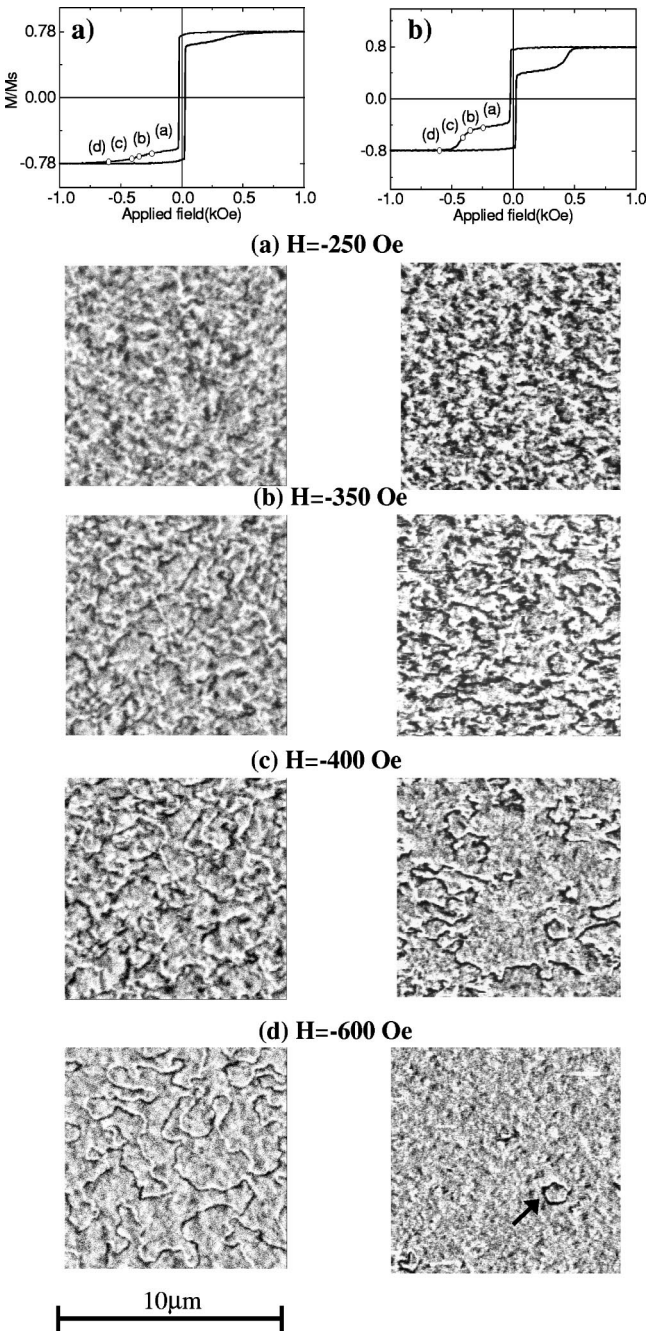

FIG. 7. MFM images on Co/Ru/Co (a) and Co/Ru/CoFe (b), showing the appearance of long connected Néel walls during the reversal of the net magnetic moment and their stability in a negative magnetic field. The main difference between Co/Ru/Co and Co/Ru/CoFe consists of a lower Q value in the CoFe case, which plays an important role in the stability of the walls. A successive set of MFM images for both Co and CoFe artificial ferrimagnets at significant fields are shown: (a) −250 Oe, (b) −350 Oe, (c) −400 Oe, (d) −600 Oe together with the corresponding *MH* curves. Black arrows point isolated stable 360° walls.

causes the magnetization inside the areas with stronger coupling to start to rotate. Large domains separated by 360° Néel-type walls appear at the end of reversal ($M/M_{\text{plateau}} = -0.90$) when most of the regions have reversed their magnetization.

The reversal mechanism of the artificial ferrimagnet net magnetic moment differs from that of a single layer by the

presence of the interlayer coupling that enhances local frictions against rotation. The development of the 360° walls is more pronounced in the AFi coupled systems than in the single films [Figs. 7(b) and Fig. 5(c)]. Fluctuations in the antiferromagnetic coupling strength and the AF duplication of the domain structure from one layer to the other, increase the density of the 360° walls. Due to the strong interlayer coupling, the features are mirrored in both AFi magnetic layers with antiparallel Néel walls. This has a strong impact on the stability of the walls. While the thick layer develops walls with centers opposite to the field direction (similar to the single layers case), in the thin layer the mirrored walls have their centers along the field direction, which makes them energetically very stable (see Appendix B). At a critical field, the wall in the thick film disappears by collapse (the center of the wall, oriented opposite to the field, shrinks). The expansion of the center part of the wall in the thin layer is prevented by the strong AF coupling with the thick layer which is oriented along the field direction. The stable walls located in the thin layer pin the walls in the thick layer due to the exchange coupling, up to fields at which the Zeeman energy overcomes the exchange.

This is consistent with the micromagnetic observations of annihilation of walls in the thick layer. Indeed, as shown in Figs. 7(c) and 7(d), the 360° walls subsist up to large fields, located in the AF plateau, for which the magnetization in wall adjacent domains is completely reversed. The field needed to annihilate the 360° Néel walls in the thick layer is inversely proportional to the Q factor[20] (which determines the relative difference between the magnetization of the two layers) because of the larger rigidity of the magnetizations when Q decreases. The MFM observations [Figs. 7(c) and 7(d)] show that the stability of the 360° walls is increased when the net moment of the AFi gets smaller. The larger density of the remaining domain walls when measured at the same field in the case of Co/Ru/Co compared to the Co/Ru/CoFe (smaller net magnetic moment in Co/Ru/Co than in the Co/Ru/CoFe) is a good indication that the total restoring torque induces a pressure on the domain wall that is proportional to the net moment.[20]

To summarize, we have shown that the reversal of the artificial ferrimagnet in the plateau occurs through the formation of 360° walls. After the reversal occurs, these walls become unstable in the thick layer and the field at which they collapse is inversely proportional to the Q factor. In contrast, in the thin layer, the walls remain very stable in the operational field window, and start to collapse at fields close to the end of the plateau. The field evolution of the domain structure governs the transport properties of the tunnel device. To test our interpretations, we have performed MR experiments in several configurations including swapping both layers, results which are reported in the next section.

V. MAGNETOTRANSPORT PROPERTIES OF TUNNEL JUNCTIONS USING ARTIFICIAL FERRIMAGNETS: IMPACT OF THE DOMAIN STRUCTURE IN THE SHAPE AND THE AMPLITUDE OF THE TMR SIGNAL

The artificial ferrimagnet system acts as a rigid block only for applied fields usually below 250 Oe, less than the operating field window [Fig. 4(a), inset concerning a minor TMR loop]. Outside this field window, the magnetization of the artificial ferrimagnet is locally disturbed and therefore no clear extended plateau could be observed in the resistance versus applied field MR curve. The shape of the MR curves is therefore strongly dependent on the microscopic magnetic characteristics of the AFi. How the local structure perturbs the MR signal is sketched in Fig. 8. The two following parameters are at the origin of the proposed scenario. First, the tunnelling current decreases exponentially with distance through the barrier. Therefore, the preferential conduction channels are the shortest paths for electrons to travel across the insulator. Because of that, the most important factor determining the magnitude of the tunneling current is the relative local orientation of the ferromagnetic moments directly across the barrier. Secondly, the TMR signal depends only on the magnetic configuration of the magnetic layers located directly at the interface with the tunnel barrier. A direct consequence of these two features is that the domains and domain walls give rise to conduction channels with different resistances determined by the lateral fluctuations of the angle between the magnetic moments of the magnetic layer in contact with the tunnel barrier. When the detection bilayer has a single domain configuration after switching, the TMR signal is only sensitive to the magnetic structure of the topmost layer of the AFi. Much effort has been put on optimizing the magnetic properties of the DL which consist of $Co_{50}Fe_{50}$(1 nm)/Fe(6 nm) bilayers. The magnetization curve of the detection bilayer shows a square loop, with a coercive field smaller than 20 Oe and the magnetization reversal takes

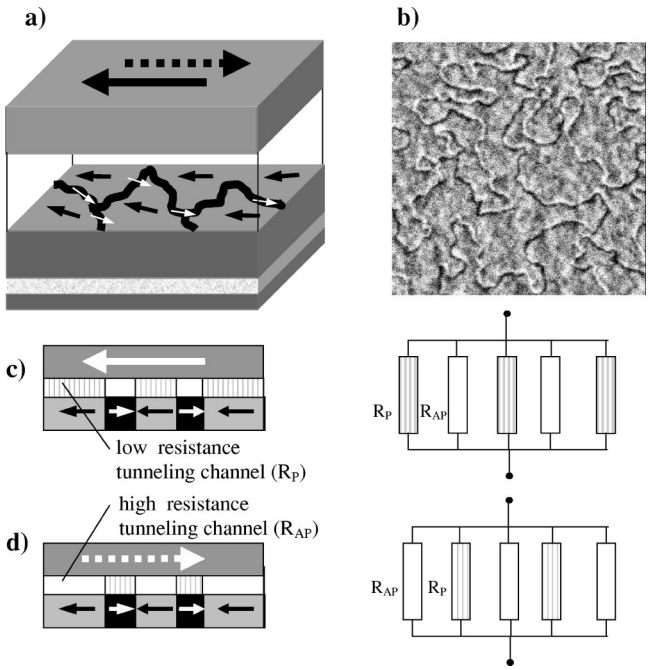

FIG. 8. (a) The influence of the 360° walls on the resistance of the MTJ sensor. (b) MFM image associated with the model displayed in (a) showing the 360° walls which appear in the top layer of the AFi during the reversal of its net magnetic moment. (c),(d) The MTJ junction is modeled by a network of in-cascade resistances determined by the different resistance conduction channels corresponding to walls and, respectively, domains as a function of the relative orientation of magnetization in detection bilayer and the top layer of the AFi system.

place in a field range less than 2 Oe.[15] Therefore, for applied fields above 30 Oe, the reversal of the detection bilayer is completed and it can be considered as being in a single-domain state. Consequently, only the magnetic state of the topmost layer of the AFi will influence the MR signal. As shown in Figs. 4(a) and 4(b) correlated with Fig. 7, the domain structure of the top layer of the AFi and especially the 360° Néel-type walls, having the magnetization in their center opposite to the magnetization of the domains, will strongly influence the amplitude and the shape of the TMR signal. While the detection bilayer forms a single domain state oriented along the direction of the field, domains separated by 360° Néel-type walls are created in the AFi during its reversal in the negative applied field. The walls in the topmost AFi layer, in contact with the tunnel barrier, give rise to high resistance channels in the tunneling process because of their antiparallel alignment of magnetization with the detection bilayer. In contrast, the magnetic domains give rise to low resistance channels [Figs. 8(c) and 8(d)] because of the parallel alignment of the local magnetization with the detection bilayer [see panel Fig. 8(c)]. The resistance of a certain spin conduction channel, determined by a region located in the top layer of the AFi where the magnetization makes an angle θ relative to the detection layer magnetization's orientation, can be estimated

$$r=\frac{1}{2}(r_P+r_{AP})+\frac{1}{2}(r_P-r_{AP})\cos(\theta), \tag{2}$$

where r_P and r_{AP} are resistances of the same spin conduction channel in a parallel ($\theta=0$) and antiparallel ($\theta=\pi/2$) configuration, respectively. Because of the existence of several spin channels, the resistance of the tunnel junction can be described by a set of parallel high and small resistances, corresponding to either a domain or a domain-wall-oriented, respectively, parallel or antiparallel to the detection bilayer. Most importantly, the situation will be totally opposite when reversing the detection bilayer from an initial magnetic state in which 360° walls are still present in the topmost layer of the AFi. In such conditions, the domains constitute conduction channels with high resistance having their magnetization oriented antiparallel with the magnetization of the detection bilayer, while the walls constitute low resistance channels [Figs. 8(c) and 8(d)]. Acting like *shortcuts*, the presence of walls will not allow the resistance of the junction to reach its maximum value.

By using the model of an in-cascade-resistances network, calculations concerning the variation of the MTJ resistance induced by 360° walls give a value of about $\Delta R/R=3.5\%$ at $H=-600$ Oe. The density of walls was estimated from the corresponding MFM image [Fig. 7(d)] and the one wall conduction channel resistance was computed by taking into account the 360° wall profile $\cos(\theta(x))$. The calculated $\Delta R/R$ is in reasonable agreement with the value extracted from the corresponding TMR curve shown in Figs. 4(a) and 4(b) ($\Delta R/R=5\%$). The difference can be attributed to local fluctuations in the orientation of magnetization inside the domains. These fluctuations are fully reflected in the MFM contrast as a *magnetic roughness* inside a domain that decreases gradually when increasing the magnetic field towards

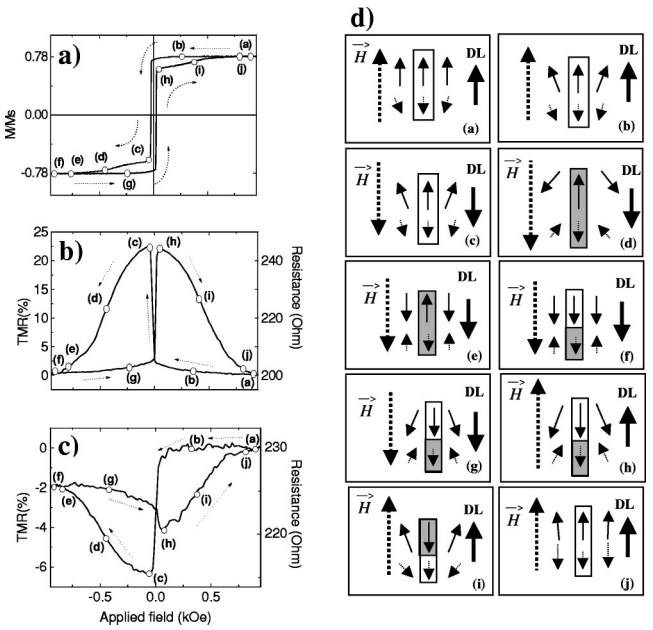

FIG. 9. Influence of the 360° walls on the shape of the TMR curve for Co/Ru/Co/Al_2O_3/CoFe MTJ. A sketch of the micromagnetic configurations for barrier adjacent magnetic layers (detection bilayer DL and the layers of the AFi stack) is presented on some significant fields in the TMR curves. (a) Magnetization curve for the Co(1.8 nm)/Ru(0.8 nm)/ Co(3 nm)/Al_2O_3/CoFe(1 nm)/Fe(6 nm) MTJ stack. (b) The TMR curve for the Co(1.8 nm)/Ru(0.8 nm)/ Co(3 nm)/ Al_2O_3/CoFe(1 nm)/Fe(6 nm) stack. The topmost layer of the AFi stack is the thicker layer. The 360° walls formed in the thick layer, during reversal, are unstable and disappear by shrinking after completion of the reversal. (c) The TMR curves is displayed for the Co(3 nm)/Ru(0.8 nm)/ Co(1.8 nm)/Al_2O_3/CoFe(1 nm)/Fe(6 nm) MTJ. Here, the topmost layer of the AFi stack is the thinner layer. In the thin layer, the 360° walls are stable in an external field, having their center oriented along the field direction, they will disappear just after leaving the AF plateau, in the flank toward saturation. (d) Sketch of the micromagnetic configurations for barrier adjacent magnetic layers (detection layer DL and the layers of the AFi stack) at some significant fields in the MH and TMR curves. *M*-*H* curves are measured on planar (reference) films grown in the same sputtering run with the wafers used for patterning junctions.

domain magnetization saturation [Figs. 7(c) and 7(d)]. These predictions have been tested in several experimental configurations as described below.

A Illustration of the domain structure effect on the TMR signal

Figures 9 and 10 summarize three different magnetic histories to illustrate the low and high resistance channels invoked by the presence of domain structure. Each figure shows the magnetization and the corresponding TMR curve, completed with a micromagnetic sketch drawn to show a view of the magnetic configuration in the tunnel junctions at some characteristic fields. In each panel, the direction of the detection bilayer (DL) and the external field are represented as well as the distribution of magnetization within the thick and the thin magnetic layers of the AFi, illustrated by the top and bottom lines of arrows, respectively. The gray areas locate the center of the 360° Néel-type wall in each of the layers.

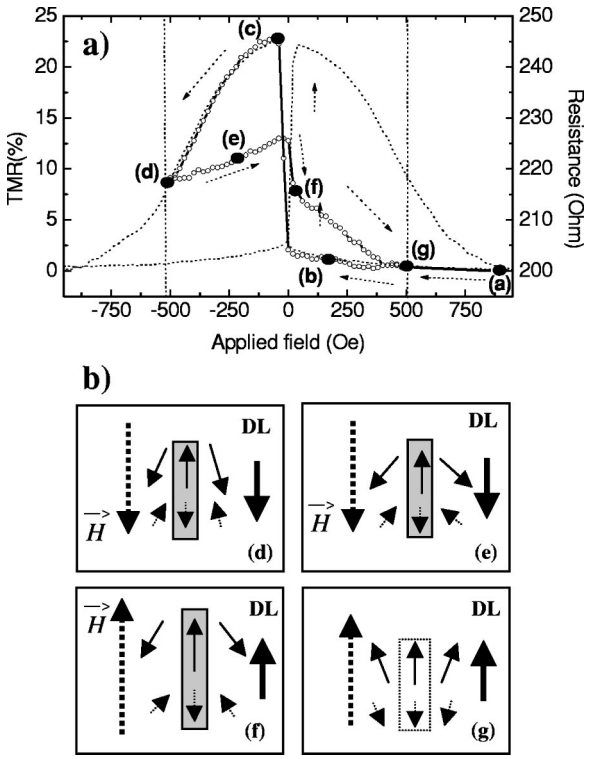

FIG. 10. (a) Minor loop and corresponding TMR curves of the Co(1.8 nm)/Ru(0.8 nm)/Co(3 nm)/Al_2O_3/ CoFe(1 nm)/Fe(6 nm) MTJ in a field range where the 360° walls are preserved in the thick layer (the reversal is not completed in negative field). The domain structure in the top layer of the AFi is clearly evidenced on the TMR signal, the walls act as high resistive channels due to their center opposite to the detection bilayer. (b) Micromagnetic sketch showing the magnetic configuration in the barrier adjacent magnetic layers (AFi and DL) at some significant values of the applied magnetic field.

1. Major loop, thick magnetic layer of AFi in contact with the tunnel barrier

Let us first consider the case where the topmost layer of the artificial ferrimagnet is the thick magnetic layer. For this purpose, the magnetization [Fig. 9(a)] and the corresponding TMR [Fig. 9(b)] curves have been measured on a Co(1.8 nm) / Ru(0.8 nm)/ Co(3.0 nm) / Al_2O_3 / CoFe(1 nm) / Fe(6 nm) magnetic tunnel junction. The thick layer is then in contact with the tunnel barrier and therefore its magnetic behavior governs the shape and amplitude of the TMR signal. Prior to the measurement, the sample was saturated in a positive applied field and therefore all magnetic layers are expected to be in a single-domain state [state (a) of Figs. 9(a), 9(b), and 9(d)]. In the AF plateau, the layers of the AFi are firmly antiferromagnetically coupled. The decrease of the positive applied field leads to the appearance of uniformly magnetized regions whose effective magnetic moments are aligned within an angle bisected by the direction of the positive saturation field [Fig. 9(d) state (b)]. These domains are separated by regions where the torque on the magnetic moments is zero defining the location of the emerging 360° walls. This magnetic state, antiferomagnetically duplicated in the thin magnetic layer by the exchange coupling, is the source of the small increase of resistance on the (a-b) branch of the M-R curve in Fig. 9(b). After the switching of the DL, corresponding to a sharp increase of resistance [Figs. 9(b) state (c) and 9(d) state (c)], the resistance decreases slowly. Indeed, the clockwise and counterclockwise rotation of the uniformly magnetized domains proceeds continuously and is mirrored in the thin magnetic layer [Fig. 9(d) state (d)]. The 360° walls formed in the thick magnetic layer during its reversal are unstable. The magnetic moment at the center of the walls [Fig. 9(d) state (e)] are oriented opposite to the field direction and disappear after completion of the topmost layer reversal [Fig. 9(d) state (f)]. However, the 360° walls formed in the thin magnetic layer during its reversal are very stable. Indeed, they have their center moments [Fig. 9(d) state (e)] oriented along the field direction. Applied fields higher than the $H_{max}=1$ kOe accessible in our experimental setup are just not strong enough to complete the saturation of the thin layer (the walls in the thin layer disappear just in the flank towards saturation). Since the thick magnetic layer is saturated in a negative applied field of $-H_{max}=-1$ kOe, its behavior on the $(-H_{max},H_{max})$ branch of the MR curve is similar than the $(H_{max},-H_{max})$ branch. So, the MR curve is symmetric. The validity of this model is further supported by additional measurements performed on a magnetic tunnel junction for which the thin layer of the AFi is in contact with the tunnel barrier.

2. Major loop, AFi thin magnetic layer in contact with the tunnel barrier

The stability of the 360° walls in the thin magnetic layer at negative applied fields of $-H_{max}=-1$ kOe is exemplified by the transport properties of Co(3 nm) / Ru(0.8 nm) / Co(1.8 nm) / Al_2O_3 / CoFe(1 nm) / Fe(6 nm) MTJ [Fig. 9(c)]. While its M-H curve is identical to the reversed case [Fig. 9(a)], the MR curve shows a large asymmetry in the signal [Fig. 9(c)]. Here, the topmost layer of the AFi stack is the thin layer and therefore its field-dependent micromagnetic structure governs the shape and amplitude of the TMR signal.

Here again, prior to measurement, the sample was saturated in a positive applied field and therefore all magnetic layers are in a single-domain state [State (a) of Figs. 9(a), 9(c), and 9(d)]. In contrast to the previous case, the resistance of the MTJ is then maximum because of the antiparallel alignment between the magnetization of the DL and the thin magnetic layer [Fig. 9(d) state (a)]. Only small fluctuations in the orientation of the magnetization, duplicated in the thin magnetic layer by the exchange coupling, explain an almost constant resistance on the (a-b) branch of the MR curve [Fig. 9(c)]. After the reversal of the DL, a sharp decrease of resistance occurs because of the parallel alignment of both adjacent layers, [Figs. 9(c) state (c) and 9(d) state (c)]. By further increasing the field, the resistance value increases slowly due to the clockwise-counterclockwise rotation of the uniformly magnetized domains in each magnetic layer of the AFi [Fig. 9(d) state (d)]. The existence and stability of the 360° walls in the thin magnetic layer up to high negative fields is demonstrated on the TMR curves which never reach the high resistance state obtained in the positive saturated state [state (a)]. As shown in Figs. 9(d) state (f) and 8(d), the walls act as low resistance channels, the direction of the center of the walls being oriented along the magnetization of the detection bilayer. By reducing the applied field,

from $-H_{max}=-1$ kOe to zero, the rotation of the uniformly magnetized domains in each magnetic layer proceeds [Fig. 9(d) state (g)] and the resistance slowly decreases. Here, the collection of parallel resistances is composed of high resistance channels (for which the magnetizations of the domains are nearly opposite to the magnetization of the DL) and by low resistance channels (for which the network of 360° domain walls have their center magnetization parallel to the magnetization of the DL) [Fig. 8(d)]. The resistance obtained at zero field depends clearly on the density of walls which remained at $-H_{max}$ [Fig. 9(d) state (g)]. In Figs. 9(c) state (h) and 9(d) state (h), the two networks of resistances are almost equivalent and therefore, the reversal of the DL gives rise to a small variation of the TMR signal. Then, the further increase of resistance is related to the rotation of the magnetization within the domains and the annihilation of the walls [Fig. 9(d) state (j)].

3. Minor loop, AFi thick magnetic layer in contact with the tunnel barrier

The process of magnetic reversal and the collapse of the unstable 360° Néel-type walls in the thick magnetic layer is exemplified in Fig. 10 using measurement of minor MR curves. We must keep in mind that in this sample the thick magnetic layer is again in contact with the tunnel barrier. The field decreasing branch of the MR curve in Fig. 10(a) is the same as in Fig. 9(b). Increasing the field in the negative direction gives a curve which is identical to Fig. 9. However, the process is not reversible. Stopping before saturation, at point (d) and decreasing the negative field towards zero, then increasing the field in the positive direction, leads to a clear irreversible change in the TMR signal. This indicates clearly that the reversal of the thick layer in point (d) is not yet completed. A network of 360° walls and fluctuations of magnetization in domains (magnetic roughness) still exists [Fig. 10(b) state (d)] in the thick layer, too. In a decreasing negative field the resistance increases gradually due to a small relaxation of magnetization in the uniformed magnetized domains towards the direction of the positive saturating field [Fig. 10(d) state (e)]. In this negative field branch, the 360° walls are stable. By reversing the field, the DL switches leading to a jump in the MR signal. At this characteristic field [panel 10(b) state (f)], the center of the 360° walls is parallel to the detection bilayer while the domains are still nearly opposite to the direction of the DL. The amplitude and especially the sign of the jump in the MR curve [state (f) of Fig. 10] is of particular importance. Indeed, a steep drop of resistance in the MR curve indicates that the switch of the DL has activated a predominant low conductive channel, associated with the network of walls. Interestingly, the conduction channels associated with the domains are of much higher resistance but do not dominate the resistive process since the resistance of the sample decreases after the switch of the DL. This irreversible process confirms the validity of the model of resistances in cascade associated to magnetic domains and domain walls.

In this paper, the existence of stable and unstable walls and their influence on the magnetoresistance of the tunnel sensor have been demonstrated. For overcoming the effects on the TMR signal of stable walls located in tunnel barrier adjacent magnetic layer, artificial ferrimagnets with a smaller Q (so a smaller gain in rigidity) have to be used in MTJ devices. However, a large coercivity for hard layers is needed because it provides a large magnetic rigidity. The alternative to obtaining high rigidity is to build AFi with single magnetic layers having large coercivities. Consequently, a given rigidity of the AFi can be reached by amplification of a larger rigidity of a single layer by a smaller Q factor (larger net magnetic moment). Therefore, the stability of the walls will be decreased. Results on systems with different amplification factors Co/Ru/Co ($Q=4$) and $Co/Ru/Co_{50}Fe_{50}$ ($Q=2$) have shown that similar rigidities are reached by starting from a higher coercivity in the case of the CoFe single layer. As shown in Fig. 7, the stability of the walls is much more pronounced in the AFi with the higher Q and its consequence is relevant on the TMR curves. The field window in which the resistance remains constant is inversely proportional with the amplification factor, for constant coercivities [Fig. 4(b)]. This result is consistent with the increase of the density of reminiscent walls at large fields for larger Q factor as shown in Fig. 7(d), which compares the situations for Co/Ru/Co and Co/Ru/CoFe samples.

VI. CONCLUSIONS

In a magnetic tunnel junction device, the spin-dependent phenomena are strongly dependent on the magnetic state of the two magnetic metal-oxide interfaces. The resistance of the junction depends on the relative orientation of the two magnetic layer magnetizations. When the magnetic layers that are in contact with the barrier form a domain structure, the resistance of the junction is strongly influenced. The reversal of the AFi was investigated in detail, supported by local MFM imaging and TMR results. We have shown that a reduction in the TMR signal is correlated with the existence of 360° walls in the AFi top layer. This leads to tunneling channels with different resistances, determined by the relative local orientation of the magnetizations in the two magnetic layers separated by the tunnel barrier. The tunneling device, having the AFi subsystem in a multidomain configuration, has been modeled by a network of resistances in cascade. Each resistance corresponds to a section in the junction containing a magnetic domain or a magnetic domain wall with a given local orientation relative to the detection bilayer. One of the most significant results of our study was the demonstration of the tunnel device as a sensitive probe for measuring small magnetic fluctuations associated with micromagnetic defects, domains, and walls. These fluctuations, which modulate the resistance of the tunnel junction are fully reflected in the shape and the amplitude of the TMR signal.

ACKNOWLEDGMENTS

The authors thank Professor R. L. Stamps and Dr. U. Ebels for illuminating discussions and critical readings of the paper. This work was supported by the European *Brite Euram*, Program Contract No. BRPR-CT95-001, the EC Framework IV Materials Technology Programme, Contract No. BRPR-CT98-0657, and the *Dynaspin* program, *Training and Mobility of Researchers* network, under Contract No. FMRX-CT97-0147. K.O. also acknowledges NSF Grant No. CNRS-9603252.

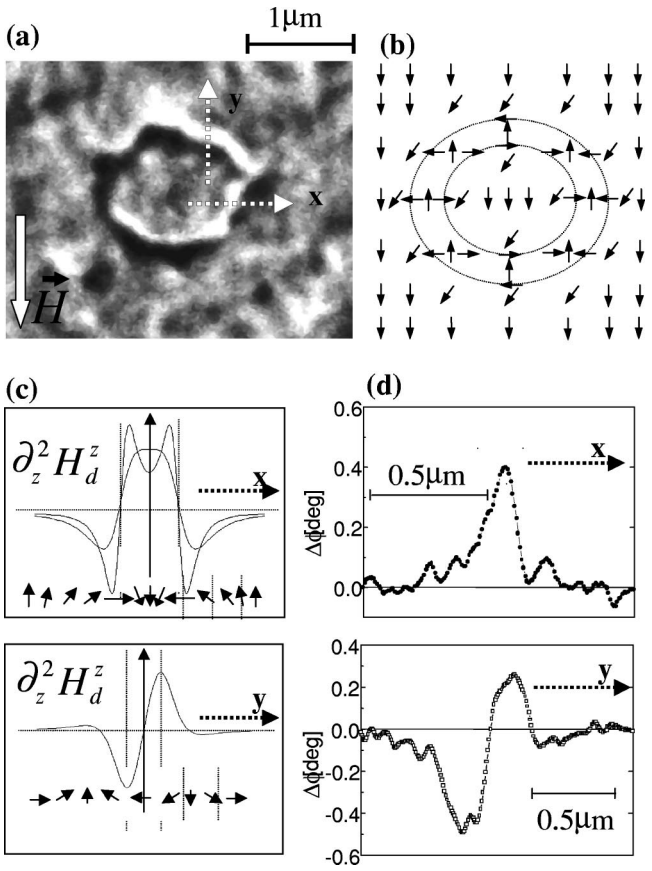

FIG. 11. Measured MFM contrast (a) and the magnetization configuration (b) for a 360° circular wall. The simulated MFM contrast, computed in two situations where the wall is either parallel or perpendicular to the field direction. (c) are in good agreement with line sections on the measured MFM images (d).

APPENDIX A: ANALYSIS OF MFM CONTRAST FOR A 360° WALL

The MFM tip, magnetized only in the z perpendicular direction, probe the second derivative of the stray field z component[30,31] in a phase detection mode.[29] Figure 11(a) presents a MFM image of a 360° circular wall that separates uniformly magnetized regions [see Figs. 5(e), corresponding to a CoFe single layer). From the associated magnetization loop (Fig. 5), we observe that the magnetization is mostly reversed at the field which corresponds to this wall profile, so all the domains have the magnetization oriented along the negative field direction. The contrast is given only by the stray field of the wall that subsists after the magnetization reversal. The magnetic structure of the wall, proposed by Heyderman *et al.*,[32] Gillies *et al.*,[33] and Cho *et al.*[36] is shown in Fig. 11(b), and can be used to explain all types of expected contrast for different 360° walls orientation, relative to the field direction and domain magnetization.

We have simulated the MFM contrast for two particular situations concerning the orientation of the wall: the wall is parallel or perpendicular to the field direction. Each configuration is defined by a certain magnetization profile[34,35] $\vec{M}(x,y,z)$:

$$\vec{M}^{\parallel}(x,y,z)=\frac{c_1^2}{c_1^2+[(x-\mu_1)/\Delta)]^2}+\frac{c_2^2}{c_2^2+[(x-\mu_2)/\Delta)]^2}, \tag{A1}$$

$$M^{\perp}(x,y,z)=c_1\arctan[(x-\mu_1)/\Delta]+c_2\arctan[(x-\mu_1)/\Delta]. \tag{A2}$$

Parameters $c_1,c_2,\mu_1,\mu_2,\Delta$ are adjusted to fit the corresponding wall profile of width Δ. In each case, the z component of the stray field H_d^z was calculated from the density of magnetic charge $\rho(x,y,z)$ corresponding to a 360° wall.

$$\rho(x,y,z)=-\nabla\cdot\vec{M}(x,y,z). \tag{A3}$$

A scalar potential ϕ, obtained from the Poisson equation

$$\Delta\phi(x,y,z)=-4\pi\rho(x,y,z), \tag{A4}$$

allows us to compute the stray field

$$H_d(x,y,z)=-\nabla\phi(x,y,z), \tag{A5}$$

and subsequently, the MFM signal proportional with $\partial^2 H_d^z/\partial z^2$. Results of the simulation [Fig. 11(c)] show a good agreement with line sections on the MFM images [Fig. 11(d)].

APPENDIX B: STABILITY OF 360° WALLS IN THE ARTIFICIAL FERRIMAGNET LAYERS

This section provides the analysis concerning the stability of 360° Néel type walls, in an artificial ferrimaget system. The total energy in an antiferromagnetically coupled system, with in-plane magnetization, submitted to an external field H, can be expressed as[37,38]

$$\begin{aligned}\varepsilon(H)=&\int\left\{A\left[t_1\left(\frac{d\theta_1}{dx}\right)^2+t_2\left(\frac{d\theta_2}{dx}\right)^2\right]\right.\\&\left.+K_L[t_1\sin^2\theta_1+t_2\sin^2\theta_2]\right\}dx\\&+\int\{J[\sin\theta_1\sin\theta_2+\cos\theta_1\cos\theta_2]\\&-MH[t_1\cos\theta_1+t_2\cos\theta_2]\}dx,\end{aligned} \tag{B1}$$

where θ_1,θ_2 describe the orientation of the magnetization in each layer relative to the field direction. The first set of terms contains the intralayer exchange (A) and local anisotropy (K_L), that determine the shape and the energy of the uncoupled domain walls in the system. The magnetostatic energies due to the divergence of the magnetization in the film plane, varying as $\sin^2\theta$ are included in K_L. The second set of terms contains the interlayer coupling energy and the Zeeman energy in an applied field H. For example, in a static configuration without any magnetic field or exchange AF coupling, the energies of independent 180° walls are $\sigma_{1,2}=4\sqrt{AK_L}$.

During the reversal of the net magnetic moment, antiferromagnetically mirrored 360° walls appear in each layer of the AFi system. To estimate the stability of these walls, a simplified model is proposed. Centered one above another, antiferromagnetically mirrored volumes in the thin and in the thick layer of the artificial ferrimagnet, are considered. In each volume we suppose a 360° wall. λ_1 and s_1 are the perimeter and the surface of the wall in the thick AFi layer (thickness t_1), and λ_2 and s_2 are the perimeter and the sur-

face of the wall in the thin layer (thickness t_2). In the thick layer the domain magnetization is oriented along the field direction and the magnetization of the center of the wall opposite to the field direction. In the thin layer the domain magnetization is opposite to the field direction, while the center of the wall has the magnetization along the field direction. The total energy of this ''two walls'' configuration $\varepsilon_2(H)$ is calculated and compared with the energy for the ''one wall'' configurations for which (i) the wall disappears in the thick layer and subsists in the thin layer $\varepsilon_1^1(H)$ or (ii) the wall disappears in the thin layer and subsists in the thick one $\varepsilon_1^2(H)$:

$$\varepsilon_2(H) = -MHS[t_1 - t_2 - 2(s_1 t_1 - s_2 t_2)] + \sigma(\lambda_1 t_1 + \lambda_2 t_2) - 2J(S/2 - s_1 + s_2), \quad \text{(B2)}$$

$$\varepsilon_1^1(H) = -MHS(t_1 - t_2 + 2s_2 t_2) + \sigma\lambda_2 t_2 - 2J(S/2 - s_2), \quad \text{(B3)}$$

$$\varepsilon_1^2(H) = -MHS(t_1 - t_2 - 2s_1 t_1) + \sigma\lambda_1 t_1 - 2J(S/2 - s_1). \quad \text{(B4)}$$

The difference in energy between the ''two wall'' and ''one wall'' configurations is

$$\Delta\varepsilon_1(H) = \varepsilon_2(H) - \varepsilon_1^1(H) = 2MHs_1 t_1 + \sigma\lambda_1 t_1 - 2J[2s_2 - s_1], \quad \text{(B5)}$$

if the wall disappears in the thick layer and subsists in the thin layer, at a given value of the applied field H. This process becomes energetically favorable when $\Delta\varepsilon_1 > 0$, true at applied fields

$$H > \frac{J[2s_2 - s_1] - \sigma\lambda_1 t_1/2}{Ms_1 t_1} = H_{xc} - H_{\text{anisotropy}}. \quad \text{(B6)}$$

The stability of the wall is determined by the balance between Zeeman + domain-wall energy (which tend to annihilate the wall in the thick layer) and the AF coupling energy (which tends to preserve the wall acting as a pinning source). The higher the coupling strength J, the higher the critical field where the wall disappears in the thick layer. The higher the local anisotropy, for a given value of J, the smaller the critical field. The larger the magnetic moment of the thick layer, the smaller the critical field, (higher pressure exerted on the wall). The values of the critical fields (extracted from MFM images by analyzing the disappearance of walls as a function of the applied field), give local measures of coupling strength and anisotropies.

If hypothetically, the wall would disappear in the thin layer and would subsist in the thick one, the variation of energy would be

$$\Delta\varepsilon_2(H) = \varepsilon_2(H) - \varepsilon_1^2(H) = -2MHs_2 t_2 + \sigma\lambda_2 t_2 - 2Js_2. \quad \text{(B7)}$$

This process is energetically unfavorable, leading to a magnetic state with a higher energy, in the field range at which 360° walls are supposed to collapse.

In conclusion, at the end of domain magnetization reversal, 360° walls exist in the two layers of the AFi system. By increasing the applied field, walls disappear in the thick layer by shrinking their center part. This occurs at a critical field which depends on the local antiferromagnetic coupling (which acts as an additional pinning parameter) and on the local anisotropy. The walls located in the thin layer are stable, having their center aligned along the field direction. For these stable walls, the Zeeman and the AF coupling energy both act as pinning sources.

[1] J.S. Moodera, L.R. Kinder, T.M. Wong, and R. Meservey, Phys. Rev. Lett. **74**, 3273 (1995); T. Miyazaki and N. Tezuka, J. Magn. Magn. Mater. **139**, L231 (1995).

[2] W.J. Gallagher, S.S.P. Parkin, Y. Lu, X.P. Bian, A. Marley, K.P. Roche, R.A. Altman, S.A. Rishton, C. Jahnes, T.M. Shaw, and G. Xiao, J. Appl. Phys. **81**, 3741 (1997).

[3] P. Grunberg, R. Schreiber, Y. Pang, M.B. Brodsky, and H. Sower, Phys. Rev. Lett. **57**, 2442 (1986).

[4] P. Bruno, Phys. Rev. B **52**, 411 (1995).

[5] K. Ounadjela, L. Zhou, R. Stamps, P. Wigen, M. Hehn, and J. Gregg, J. Appl. Phys. **79**, 4528 (1996).

[6] Z. Zhang, L. Zhou, P. Wigen, and K. Ounadjela, Phys. Rev. B **50**, 6094 (1994).

[7] S.S.P. Parkin, N. More, and K.P. Roche, Phys. Rev. Lett. **64**, 2304 (1990).

[8] D.M. Edwards, J. Mathon, R. Muniz, and S. Phan, J. Phys.: Condens. Matter **3**, 4941 (1991).

[9] N. Persat, H.A.M. van den Berg, and A. Dinia, J. Magn. Magn. Mater. **165**, 446 (1997).

[10] S.S.P. Parkin, Phys. Rev. Lett. **67**, 3598 (1991).

[11] S. Zoll, A. Dinia, D. Stoeffler, M. Gester, H.A.M. Van den Berg, and K. Ounadjela, Europhys. Lett. **39**, 323 (1997).

[12] S. Zoll, A. Dinia, H.A.M. van den Berg, J.P. Jay, C. Mny, G. Pan, A. Michel, V.P. Bohnes, and P. Panissod, Phys. Rev. B **57**, 4842 (1998).

[13] A spurious geometrical enhancement of the TMR effect is likely to occur if the resistance of the barrier is too small as compared to that of the current leads. See, e.g., R.M.J. van de Verdoonk, J. Nowak, R. Meservey, J.S. Moodera, and W.J.M. de Jonge, Appl. Phys. Lett **71**, 2839 (1997).

[14] J.H. Greiner, J. Appl. Phys. **42**, 5151 (1971).

[15] C. Tiusan, M. Hehn, K. Ounadjela, Y. Henry, J. Hommet, C. Meny, H.A.M. van den Berg, L. Baer, and R. Kinder, J. Appl. Phys. **8**, 5276 (1999).

[16] J.S. Moodera, E.F. Gallagher, K. Robinson, and J. Nowak, Appl. Phys. Lett. **70**, 3050 (1997).

[17] M. Julliere, Phys. Lett. **54A**, 225 (1975).

[18] L. Baer (private communication).

[19] K. Ounadjela, L. Zhou, P. Wigen, R. Stamps, and J. Gregg, Europhys. Lett. **39**, 213 (1997).

[20] H.A.M. van den Berg, W. Clemens, G. Gieres, G. Rupp, M. Vieth, J. Wecker, and S. Zoll, J. Magn. Magn. Mater. **165**, 524 (1997).

[21] The M-H curves [Fig. 2(b) corresponding to the Co/Ru/Co and

Fig. 3(b) corresponding to the case of Co/Ru/CoFe artificial ferrimagnets] allow us to estimate the experimental values Q_{exp} by comparing the AFi coercivity with the coercivity of the single Co or CoFe layers. The experimental gains in rigidity ($Q_{exp}=3$ in the Co/Ru/Co AFi and $Q_{exp}=2$ in the Co/Ru/CoFe) are smaller than the theoretical predictions ($Q=4$), computed from the previous definition relation between Q and the magnetic moments of each AFi layer (m_1 and m_2). One reason is an unequal intermixing degree for the Co and CoFe at the Co/Ru and CoFe/Ru interfaces. Co will lose magnetic moment at the interface with Ru and Al oxide while the $Co_{50}Fe_{50}$ is preserving its ''as deposited magnetic moment'' due to a low intermixing degree at the interfaces. Consequently the experimental values for m_1 and m_2 in each of the two AFi systems are not equal with the theoretical estimations by taking into account the sputtered thicknesses.

[22] P. Panissod, in *Frontiers in Magnetism of Reduced Dimension Systems*, Vol. 49 of *NATO Advaced Study Institute, Series 3: High Technology*, edited by V. G. Bar'yakhtar, P. E. Wigen, and N. A. Lesnik (Kluwer, Dordrecht, 1998).

[23] H.W. Fuller and M.E. Hale, J. Appl. Phys. **31**, 238 (1960).

[24] K.D. Laver, Thin Solid Films **2**, 149 (1968).

[25] K.J. Harte, J. Appl. Phys. **39**, 1503 (1997).

[26] H. Herzer, IEEE Trans. Magn. **25**, 3327 (1989).

[27] R.J. Spain and I.B. Puchalska, J. Appl. Phys. **35**, 824 (1968).

[28] D.V. Berkov and N.L. Gorn, Phys. Rev. B **57**, 14 332 (1998).

[29] H.N. Lin, Y.H. Chiou, B.M. Chen, H.P.D. Shieh, and C.R. Chang, J. Appl. Phys. **83**, 4997 (1998).

[30] J.J. Saenz, N. Garcia, and J.C. Zlonczewski, Appl. Phys. Lett. **53**, 1449 (1998).

[31] D. Rugar, H.M. Mamin, P. Guethner, S.E. Lambert, J.E. Starn, I. McFadyen, and T. Yogi, J. Appl. Phys. **68**, 1169 (1990).

[32] L.J. Heydermann, J.N. Chapmann, and S.S.P. Parkin, J. Magn. Magn. Mater. **96**, 125 (1991).

[33] M.F. Gillies, J.N. Chapman, and J.C.S. Kools, J. Appl. Phys. **78**, 5554 (1995).

[34] A. Hubert, W. Rave, and S.L. Tomlinson, Phys. Rep. **258**, 173 (1995).

[35] R.I. Potter, J. Appl. Phys. **41**, 1648 (1970).

[36] H.S. Cho, C. Hou, M. Sun, and H. Fujikawa, J. Appl. Phys. **85**, 5160 (1999).

[37] R.L. Stamps, A.S. Carrico, and P.E. Wigen, Phys. Rev. B **55**, 6473 (1997).

[38] R.L. Stamps, Phys. Rev. B **49**, 339 (1994).